Buoyant Forcing within the Marine Stratocumulus-topped Boundary Layer

KERRY A. MOYER AND GEORGE S. YOUNG

Department of Meteorology, The Pennsylvania State University, University Park, Pennsylvania

(Manuscript received 8 April 1991, in final form 7 December 1992)

ABSTRACT

A marine stratocumulus experiment was conducted off the coast of southern California during June and July 1987 as part of the First ISCCP (International Satellite Cloud Climatology Project) Regional Experiment (FIRE). This investigation addresses the FIRE goal of enhancing our understanding of the buoyant production/destruction of turbulent kinetic energy within the marine stratocumulus-topped boundary layer through an analysis of the vertical profiles of buoyancy flux collected by the NCAR Electra aircraft. The FIRE boundary layers were observed to span the range of buoyant forcing possibilities from nearly pure surface-forced convection through nearly pure cloud top–forced convection.

1. Introduction

The marine stratocumulus–topped boundary layer is a very common phenomenon, particularly over the cool ocean currents that are prevalent along the western coastline of continents. Although several ambitious field experiments have focused on this complex type of boundary layer, its turbulent structure is still enigmatic in many ways. The Marine Stratocumulus Experiment (STRATEX) (Brost et al. 1982a,b; Albrecht et al. 1985; and Penc and Albrecht 1987) and the Dynamics and Chemistry of Marine Stratocumulus (DYCOMS) Experiment (Kawa and Pearson 1989) were both conducted off the California coast. The Joint Air–Sea Interaction Experiment (JASIN), on the other hand, was conducted in stratocumulus over the North Sea (Pollard 1978). This region was also the site of studies by Nicholls (1984, 1989), Nicholls and Leighton (1986a), and Nicholls and Turton (1986b). These studies have identified surface buoyancy flux, cloud-top entrainment flux, cloud-top infrared cooling, and differential sensible and latent heating of the cloud and subcloud layers as potentially influential in determining the profile of buoyant forcing exhibited by a particular stratocumulus-topped PBL.

The purpose of this investigation is to shed additional light on the patterns of buoyant forcing observed within the marine stratocumulus-topped boundary layer using turbulence data collected during the marine stratocumulus portion of FIRE. A thorough review of the research objectives of this experiment can be found in Albrecht et al. (1988). The instrumentation and the preprocessing techniques used to generate the eddy correlation turbulence statistics cited in this investigation are discussed in section 2. Section 3 examines the vertical transfers of temperature and moisture that interact to produce the wide range of features exhibited within the FIRE buoyancy flux profiles.

2. Experimental details, instrumentation, and data preprocessing

The stratocumulus portion of FIRE was conducted off the coast of California during June and July 1987. The National Center for Atmospheric Research (NCAR) Electra aircraft conducted ten flights during the field experiment. Each flight consisted of a series of turbulence legs along with periodic sounding legs. Each turbulence leg was between 35 and 70 km in length and was flown at a constant altitude. These turbulence legs were executed at various heights within the boundary layer. Table 1 contains a brief summary of important details surrounding each of the ten FIRE flights. Note that local time over the FIRE region was seven hours behind UTC. Further specifics concerning the FIRE flight operations can be found in Kloesel et al. (1988).

The turbulence data presented in this paper were collected using fast-response instrumentation (20 Hz) aboard the Electra. Air temperature was measured using a Rosemount model 102E2AL non-deiced sensor. The resolution of this instrument is 0.006°C and its accuracy is ±0.5°C. We chose to use this sensor because it was not as adversely affected by wetting problems within cloud as were the other fast-response temperature sensors at our disposal on board the Electra (Betts

Corresponding author address: Dr. Kerry A. Moyer, Department of Meteorology, The Pennsylvania State University, College of Earth and Mineral Sciences, 503 Walker Building, University Park, PA 16802-5013.

TABLE 1. A general summary of mean conditions encountered during the FIRE turbulence flights flown by the NCAR Electra, where SST is sea surface temperature, z_b is height of the stratocumulus cloud base, z_i is boundary-layer depth, $q_l$max is the maximum leg-averaged liquid-water content measured on the flight, and T_{45} and $|V_{45}|$ are air temperature and horizontal wind speed measured at 45 m.

Flight	Date (mo/d/yr)	Time (UTC)	Lat (deg)	Long (deg)	SST (°C)	T_{45} (°C)	$\|V_{45}\|$ (m s^{-1})	z_b (m)	z_i (m)	$q_l$max (g m^{-3})
1	6/29/87	1956–2234	30.8N	124.7W	17.7	15.9	5.7	800	1020	0.27
2	6/30/87	1918–2306	30.8N	122.3W	17.8	15.5	4.4	600	915	0.29
3	7/03/87	0135–0528	31.2N	122.1W	17.1	16.4	9.8	620	855	0.29
4	7/05/87	1801–2233	31.9N	121.7W	16.8	15.4	11.2	530	915	0.25
5	7/07/87	1911–2154	31.6N	122.0W	16.2	16.1	13.1	400	650	0.21
6	7/10/87	1916–2130	36.0N	125.0W	14.7	14.6	10.7	460	715	0.29
7	7/11/87	1746–2039	31.0N	124.2W	17.9	15.6	6.3	520	940	0.33
8	7/14/87	1950–2126	31.2N	123.8W	18.6	15.9	7.2	460	790	0.30
9	7/16/87	1655–1940	33.4N	119.8W	16.0	14.5	1.5	450	790	0.28
10	7/18/87	1217–1626	31.5N	121.8W	17.1	15.3	7.5	850	1150	0.21

and Boers 1990). Sea surface temperature was measured by a Barnes PRT-5 downward-looking radiometer with 0.005°C resolution and ±1.0°C accuracy.

An NCAR LA-3 Lyman-α hygrometer was used to measure absolute humidity (Buck 1976). The resolution of this instrument is ±0.2% and its accuracy is 5%. The Lyman-α may sometimes give erroneous values in cloud due to a wetting problem (Lenschow et al. 1988). The only alternative to using Lyman-α data within cloud, however, is to assume that the value of specific humidity is identical to its corresponding saturation value at that temperature. The validity of this assumption is dubious, especially near cloud boundaries where subsaturated pockets of air most certainly exist (Nicholls and Leighton 1986a). Thus, the authors have chosen to use the Lyman-α data in this investigation in lieu of imposing the saturation assumption.

Liquid water data were collected by both a Particle Measuring Systems (PMS) CSIRO (King) liquid water probe and a PMS Forward Scattering Spectrometer Probe (FSSP). The former has an apparent zero-offset problem, while the latter has a tendency of underestimating the liquid water content by as much as a factor of 2 (Paluch and Lenschow 1991). Despite the inadequacies associated with both of these instruments, the turbulent fluctuations of liquid water obtained from the two are surprisingly well correlated, as shown in Fig. 1. Furthermore, quantitatively speaking, the contribution of liquid water to the overall buoyancy flux is minimal in the stratocumulus-topped boundary layers investigated during FIRE. Specifically, the inclusion of liquid water loading reduced the buoyancy flux within the FIRE cloud layers by an average of only 7%.

Secure in the knowledge that the use of data obtained from either probe would not substantially alter the buoyancy flux profiles presented within this paper, the authors chose to use the data obtained from the CSIRO (King) probe. Before employing the data from the CSIRO (King) probe, however, the zero-offset problem was reduced by subtracting the mean liquid water content measured on the clear-air turbulence legs (i.e., 0.0975 g m^{-3}) from the liquid water content measured on the in-cloud turbulence legs.

Vertical wind was measured using a Rosemount 858 gust probe in combination with an inertial navigation system. This method of measuring turbulent fluctuations in vertical velocity appears to have worked quite well with a few notable exceptions. The gust probe may have recorded some erroneous fluctuations on those legs that repeatedly entered and exited cloud (Paluch and Lenschow 1991). Those legs exhibiting this behavior were eliminated from consideration.

Prior to eddy correlation analysis, the raw turbulence data were despiked by eliminating any data point that deviated by more than four standard deviations from the leg average. A linear detrending routine was then applied to each turbulence leg in order to minimize the mesoscale contribution in each variable. Any leg that recurringly sampled both clear air and cloudy air was eliminated from consideration. This action was

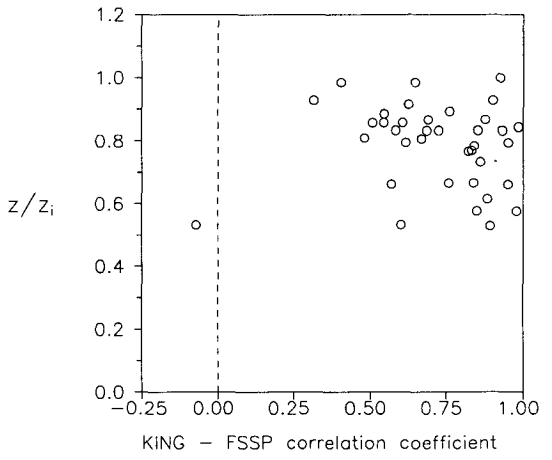

FIG. 1. The linear correlation coefficient of turbulent fluctuations in liquid water content between the CSIRO (King) probe and the FSSP for each of the in-cloud turbulence legs flown during FIRE.

taken to ensure that each turbulence leg included within the dataset was reflective of a homogeneous environment.

Two of the eddy correlation fluxes were derived using approximations that are not trivial and are presented below. Note that all of the overbars appearing in the following approximations represent mean values representative of a given turbulence leg. The vertical flux of specific humidity, $\overline{w'q'_v}$, was obtained by employing the following approximation:

$$\overline{w'q'_v} \approx \frac{1}{\bar{\rho}} \{[(\bar{r}/\bar{T})\overline{w'T'}] + \overline{w'r'}\}, \quad (1)$$

where $\bar{\rho}$ is the mean density, $\bar{r}$ is the mean absolute humidity, $\bar{T}$ is the mean temperature, $\overline{w'T'}$ is the vertical flux of temperature, and $\overline{w'r'}$ is the vertical flux of absolute humidity. The vertical flux of virtual temperature, $\overline{w'T'_v}$, which is often referred to as the buoyancy flux, was then approximated in the following manner:

$$\overline{w'T'_v} \approx \overline{w'T'}*[1 + (0.61\overline{q_v}) - \overline{q_l}] + [\bar{T}*[(0.61\overline{w'q'_v}) - \overline{w'q'_l}]], \quad (2)$$

where $\overline{w'q'_l}$ is the vertical flux of specific liquid water, $\overline{q_v}$ is the mean specific humidity, $\overline{q_l}$ is the mean specific liquid water content, and 0.61 is a dimensionless constant. The triple products $\overline{w'T'q'_v}$ and $\overline{w'T'q'_l}$ were excluded in the calculation of the buoyancy flux as these two terms were estimated to be at least an order of magnitude smaller than the remaining terms appearing in the approximation.

3. Observations

Vertical profiles of buoyancy flux measured on each of the ten flights conducted by the NCAR Electra during FIRE are displayed in Fig. 2. The buoyancy flux is directly proportional to the buoyant production and destruction of turbulent kinetic energy (TKE). Hence, the turbulent structure of the convective planetary boundary layer is dependent upon vertical variations in this buoyant production and destruction of TKE.

Three features routinely appear within the FIRE buoyancy flux profiles. These features are clearly evident in Fig. 3, which represents a layer-averaged profile of $\overline{w'T'_v}$ over all ten FIRE flights. Even the most cursory analysis of Fig. 3 reveals two positive local maxima in $\overline{w'T'_v}$, one of which is located near the sea surface and the other near cloud top. A few of the FIRE boundary layers exhibit only one of these maxima and thus, are driven almost exclusively by either surface or cloud-top boundary forcing. However, a majority exhibit both maxima and, thus, are driven by a combination of surface and cloud-top buoyant forcing. In many cases, the two forcing regimes are clearly separated by a midlevel minimum in $\overline{w'T'_v}$. This minimum generally contains near-zero or even negative values of $\overline{w'T'_v}$ and is located in the vicinity of the stratocumulus cloud base.

a. *Positive local $\overline{w'T'_v}$ maximum near the sea surface*

Sea surface temperatures in the FIRE staging area, although cool, were still generally warmer than the mean air temperatures measured on the lowest level (~45 m) turbulence legs. Exceptions to this generalization occurred on flights 5 and 6, where the sea surface temperature was at times cooler than the overlying air. The correlation between this air–sea temperature contrast at the surface and the vertical flux of temperature at 45 m for all ten FIRE flights is displayed in Fig. 4.

Vertical profiles of $\overline{w'T'}$ measured during FIRE for the boundary layer as a whole are shown in Fig. 5. Flights 1, 3, 4, 7, 8, and 10 display a positive temperature flux near the sea surface, while both positive and negative values of $\overline{w'T'}$ are observed on flights 2 and 5, and exclusively negative values of $\overline{w'T'}$ are observed on flights 6 and 9. Overall, the temperature fluxes measured at 45 m agree quite well with the bulk aerodynamic concept of local mixing down the mean surface layer gradient. There are a few notable exceptions, however. For instance, the negative temperature fluxes observed at 45 m on flights 2 and 9 are somewhat enigmatic in terms of air–sea temperature differences. This discrepancy, however, may well be caused by the presence of small-scale variations in sea surface temperature that can have a significant effect on the low-level temperature flux but are masked by the averaging technique employed to estimate the mean sea surface temperature.

The vertical distribution of water vapor within the lower portion of the marine stratocumulus-topped PBL is also profoundly influenced by the presence of the sea surface. In the absence of precipitation, the observed air–sea vapor pressure difference is the primary control on the vertical flux of specific humidity within the subcloud layer. The mean specific humidity decreases with height from the saturation value it assumes at the oceanic interface. The presence of this negative mean specific humidity gradient within the lower portion of the boundary layer promotes the development of a positive flux of specific humidity, $\overline{w'q'_v}$. Profiles of the vertical flux of water substance collected during FIRE are shown in Fig. 6. All of the marine stratocumulus-topped boundary layers investigated during FIRE exhibit positive values of $\overline{w'q'_v}$ within the lower portion of the boundary layer.

The combination of both a positive temperature flux and a positive specific humidity flux within the lowest levels of the boundary layer is indicative of turbulent eddies driven by both sensible heating and evaporation from the sea surface. This situation was the norm in most of the FIRE boundary layers. Consequently, a positive local $\overline{w'T'_v}$ maximum was commonly observed

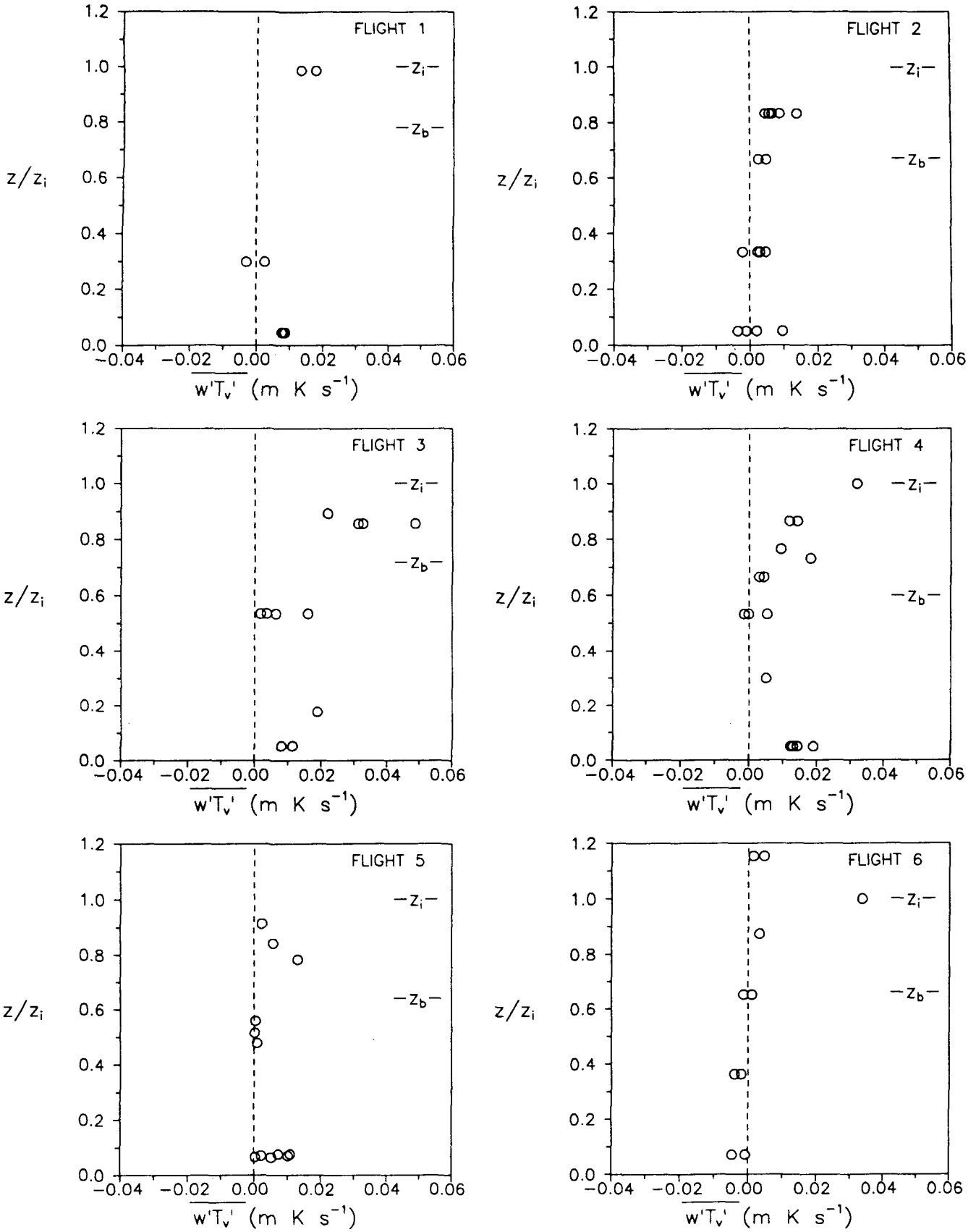

FIG. 2.

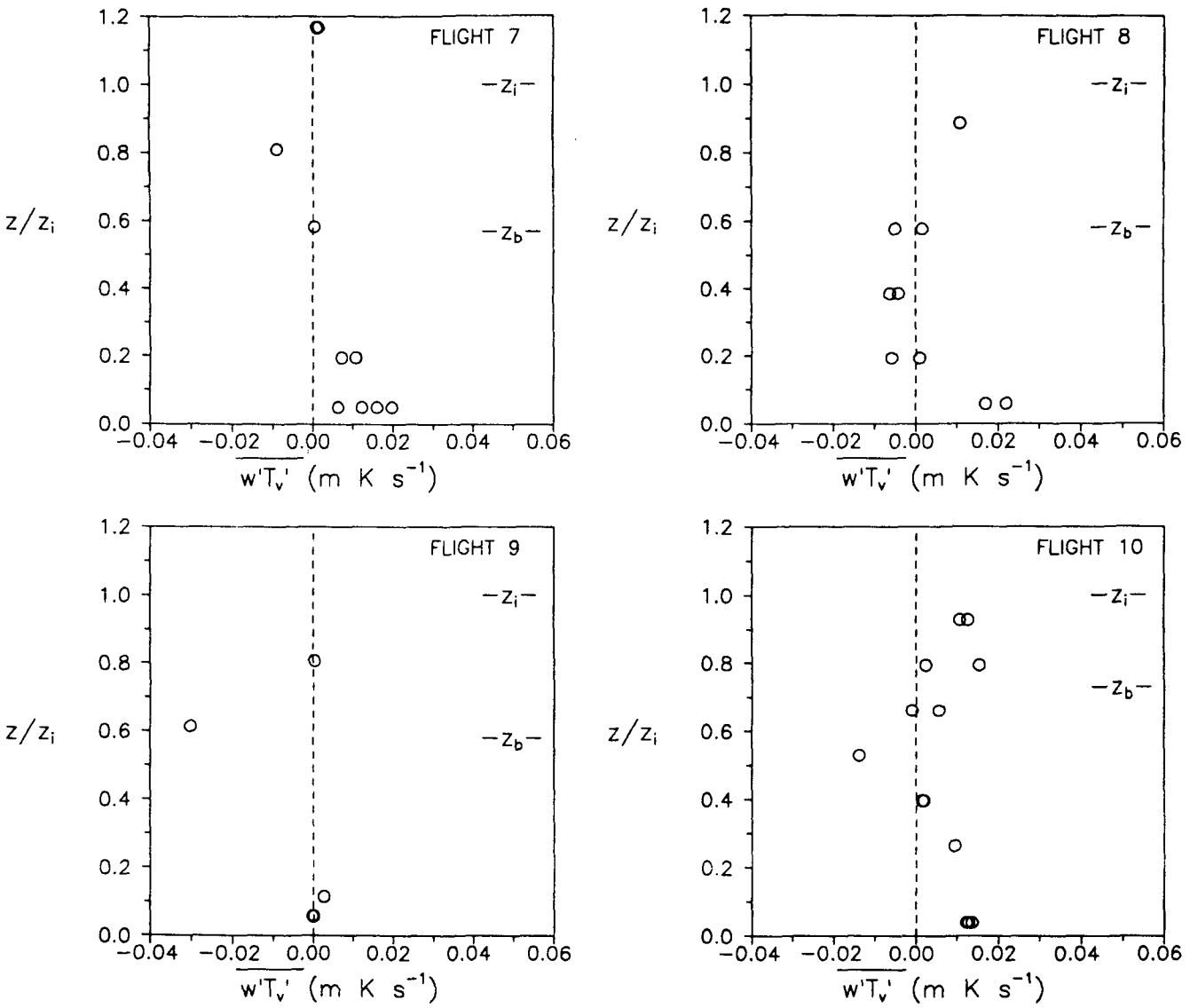

FIG. 2. Profiles of the vertical flux of virtual temperature as a function of height divided by boundary layer depth observed on FIRE flights 1–10.

near the sea surface on many of the FIRE flights. However, as previously noted, some of the turbulence legs on flights 2, 5, 6, and 9 exhibit a negative flux of temperature and a positive flux of specific humidity within the lowest levels of the PBL. On flight 5, these fluxes combined to produce a small, but positive low-level $\overline{w'T_v'}$ indicative of TKE production. On flights 2 and 9, the low-level buoyancy flux fluctuated around zero, while on flight 6, $\overline{w'T_v'}$ was negative, reflective of a sink of TKE near the surface. In summary, both the surface heat flux and the surface humidity flux played a significant role in determining both the sign and the magnitude of the buoyancy flux observed within the lower portion of the FIRE boundary layers.

b. Positive local $\overline{w'T_v'}$ maximum near cloud top

The buoyant production and destruction of TKE within the stratocumulus cloud layer is influenced by both the radiative structure of the cloud and by entrainment. Therefore, the buoyancy flux exhibited within the cloud layer should be a function of not only the mean temperature and moisture (i.e., vapor and liquid) fields within the cloud layer itself but also the temperature and moisture characteristics of the overlying capping inversion.

As shown in Fig. 3, the buoyancy flux is observed to increase with height within the cloud layer on many of the FIRE flights reaching a positive, local maximum

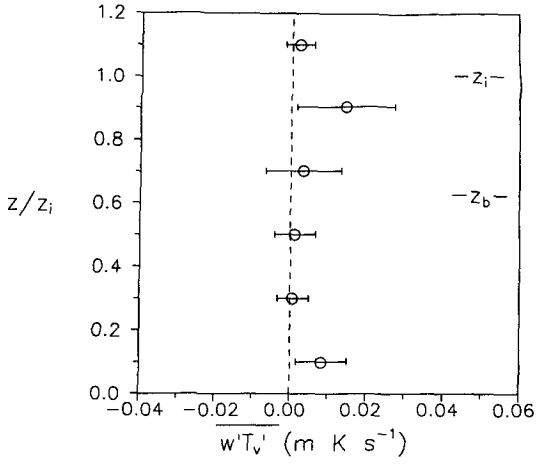

FIG. 3. The layer-averaged profile of the vertical flux of virtual temperature over all ten FIRE flights using six equispaced vertical layers of 0.2 z/z_i thickness. Horizontal bars indicate the standard deviation of $\overline{w'T'_v}$ within each layer.

near cloud top. A local cloud-top maximum in $\overline{w'T'_v}$ has been observed in past investigations of the marine stratocumulus-topped boundary layer and appears to be a common feature within this type of PBL (Nicholls and Leighton 1986a; Nicholls 1989). This cloud-top maximum in buoyant forcing can be at least partially attributed to the radiative structure of the stratocumulus cloud layer.

The radiative structure of daytime marine stratocumulus clouds is characterized by a relatively thin layer of net radiative cooling near cloud top and a net radiative warming throughout the remainder of the cloud (Nicholls 1984). In this radiative environment, turbulent eddies will transport heat down the gradient of radiative flux convergence inducing a positive temperature flux within the cloud. Therefore, taken in isolation, the radiative structure of stratocumulus clouds will tend to promote positive values of $\overline{w'T'_v}$ within the cloud layer, with a local maximum occurring near cloud top in proximity to the height of the greatest gradient in radiative flux convergence.

It is also necessary to consider the possible effects that entrained inversion layer air may have upon the buoyancy flux profile observed within the cloud (Lilly 1968; Randall 1980; Deardorff 1980a). Siems et al. (1990) have investigated the potential effects of entrainment within the FIRE boundary layers. They have concluded that the entrainment of lower equivalent potential temperature air into the FIRE boundary layers may have contributed to a positive flux of both temperature and specific humidity within cloud on many of the flights. These positive values of $\overline{w'T'}$ and $\overline{w'q'_v}$ would have in turn promoted positive values of $\overline{w'T'_v}$ within the cloud layer.

While longwave radiative cloud-top cooling and entrainment are both potential contributors to the positive local maximum in the buoyancy flux observed near cloud top in many of the FIRE boundary layers, the relative contributions made by each of these processes to this cloud-top buoyant forcing maximum cannot be ascertained on a flight-by-flight basis. This shortcoming of the FIRE dataset arises because the flight levels specified in the project design do not facilitate a study of the entrainment physics nor the radiative profiles as-

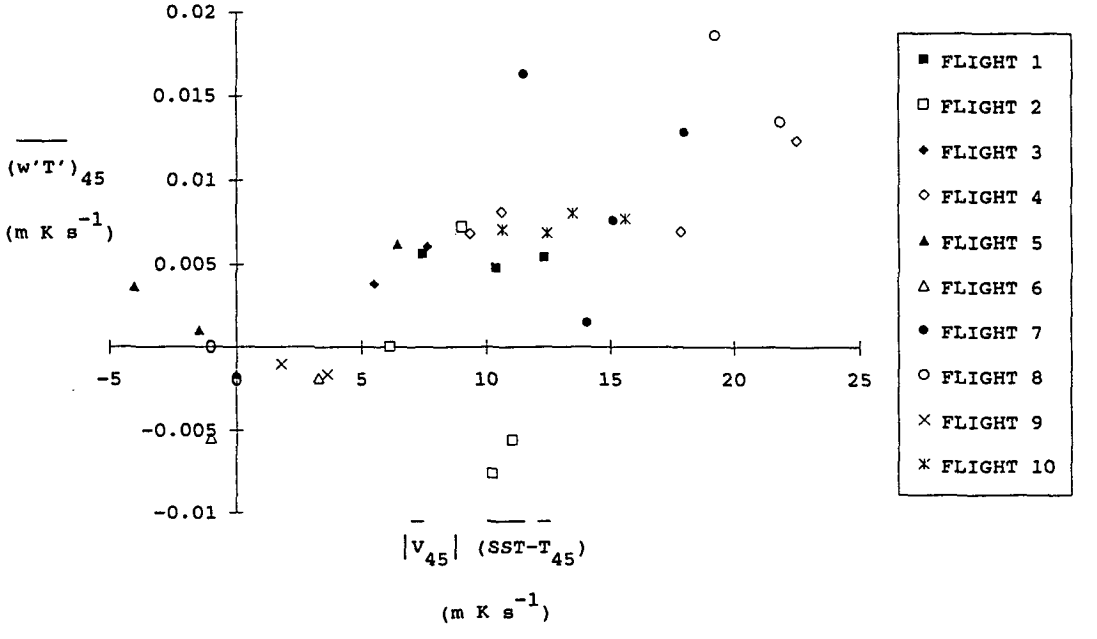

FIG. 4. The vertical flux of temperature measured at 45 m as a function of $[|\bar{V}_{45}|(\overline{SST} - \bar{T}_{45})]$.

sociated with these stratocumulus-topped boundary layers.

Although radiative cloud-top cooling may combine with entrainment to produce a positive flux of both temperature and specific total water on the vast majority of the in-cloud turbulence legs flown during FIRE, a few exceptions are apparent. For instance, three turbulence legs flown near cloud top on flights 4, 6, and 10 exhibit a positive flux of temperature in tandem with a negative flux of specific total water. This negative $\overline{w'q'_T}$ arises from negative fluxes of both water vapor and liquid water. It is somewhat surprising to find a negative total water flux in such close proximity to the hydrolapse associated with the inversion layer. Consequently, these negative values of $\overline{w'q'_v}$ and $\overline{w'q'_l}$ merit some additional consideration.

Although a linear detrending routine had been applied to the data during preprocessing with the intent of reducing the mesoscale contribution within the fluxes, a high-pass filter with a 6-km cutoff was subsequently employed to these three turbulence legs to determine whether these negative fluxes were truly microscale turbulence and not simply the product of a mesoscale circulation. While the magnitude of the filtered $\overline{w'q'_v}$ and $\overline{w'q'_l}$ were reduced in all three cases, both fluxes remained negative, indicating that a portion of each can be directly attributed to microscale turbulence.

Under certain conditions, mixing between inversion and boundary-layer air could conceivably produce a negative flux of water vapor via evaporation of liquid water near cloud top. Such mixing, however, would not result in a negative liquid water flux.

Deardorff (1980a) also observed a downward flux of water vapor near cloud top during AMTEX and linked these negative fluxes to a sampling uncertainty. Deardorff asserts that a given turbulence leg may miss the large positive contribution to $\overline{w'q'_v}$ from isolated updrafts and only sample the more prevalent negative contribution to $\overline{w'q'_v}$ from the more widespread subsidence of air back into the boundary layer.

Thus, while the negative flux of specific humidity may be attributed to either evaporative mixing or undersampling, the negative flux of liquid water can only be explained in terms of either undersampling or instrument error. In any event, the positive temperature flux observed on these cloud-top legs was large enough to dominate over the anomalous negative, specific total water flux, resulting in a positive buoyancy flux and a production of TKE on all three of these turbulence legs.

c. *Cloud-base $\overline{w'T'_v}$ minimum*

The presence of surface and cloud-top local buoyancy flux maxima on flights 1, 2, 3, 4, 5, 8, and 10 indicates that convective mixing was maintained by a combination of surface-driven and cloud top–driven convection. On these flights, the flux contribution from both the surface and cloud top–driven eddies is observed to diminish as one approaches the midlevels of the boundary layer. This minimum in buoyancy flux at the cloud base is commonly observed within marine stratocumulus-topped boundary layers (Nicholls 1984; Kawa and Pearson 1989) and is a persistent feature within large-eddy simulations (LES) of this type of PBL as well (Deardorff 1980b; Moeng 1986).

The propensity of differential latent heating within the lower portion of the cloud to produce a $\overline{w'T'_v}$ minimum at cloud base has been demonstrated numerically by both Deardorff (1980b) and Moeng (1986). In the presence of a positive moisture flux, the relatively moist updrafts tend to possess a lower lifting condensation level (LCL) than the relatively dry downdrafts. Thus, the updrafts begin to experience latent heating below the downdraft LCL, gain buoyancy relative to the downdrafts, and consequently produce a local minimum in the buoyancy flux profile just below cloud base. The base of the main stratocumulus cloud deck during FIRE was located at $0.65\ z_i \pm 0.08\ z_i$.

Differential latent heating in the vicinity of the cloud base is not solely responsible for the buoyancy flux minimum observed on the majority of FIRE flights. Many of the flights exhibit a buoyancy flux minimum containing negative values of $\overline{w'T'_v}$, whose existence may be linked to a local reversal in the mean potential temperature and/or mean specific humidity gradient near cloud base. All but one of the ten FIRE flights were flown during daylight and hence were subject to shortwave heating. The notable exception was flight 3, which was conducted during the evening. Differential shortwave heating of the cloud and subcloud layer is capable of producing such an intervening stable layer, as discussed by Nicholls (1984). The turbulent mixing of this positive potential temperature gradient may well be responsible for the negative temperature fluxes observed below cloud base on many of the FIRE flights.

Precipitation-induced evaporational cooling may also have contributed to the negative values of $\overline{w'T'_v}$ exhibited near cloud base in some of the FIRE boundary layers. Light precipitation was encountered within the subcloud layer on flights 2, 7, 8, and 9 (Laufersweiler and Kloesel 1991). Brost et al. (1982b) suggest that the latent cooling induced by the evaporation of precipitation within the subsaturated air below cloud base can lead to a net cooling of the subcloud layer relative to the cloud layer. Thus, this latent cooling can also potentially increase the stability near cloud base. Moreover, if significant evaporation was occurring below cloud base, then one would expect the mean specific humidity of the ambient air at this height to increase locally from its background value below cloud base leading to a local reversal of the mean specific humidity gradient below cloud base. Evidence of such a reversal is indeed provided by the negative fluxes of

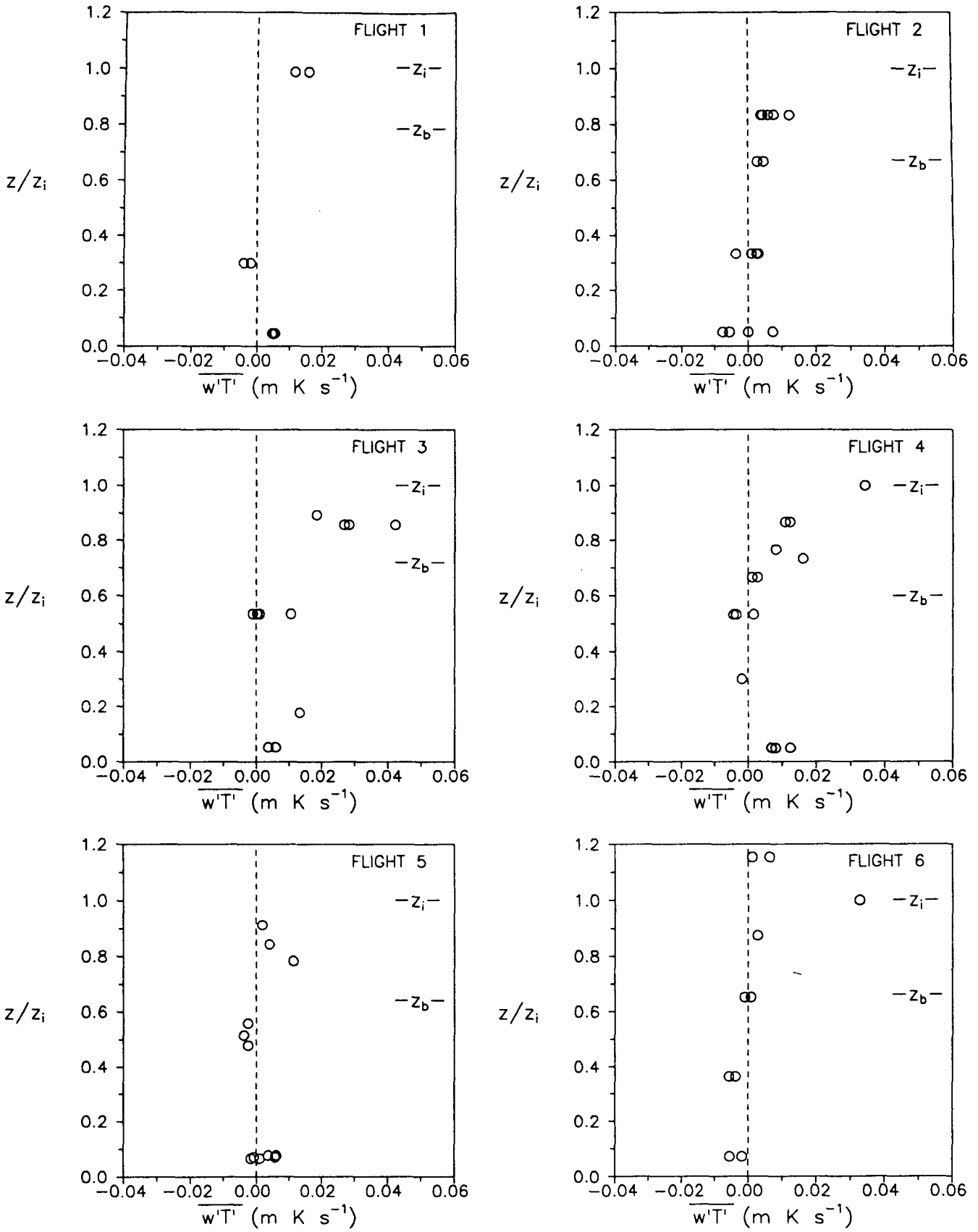

FIG. 5.

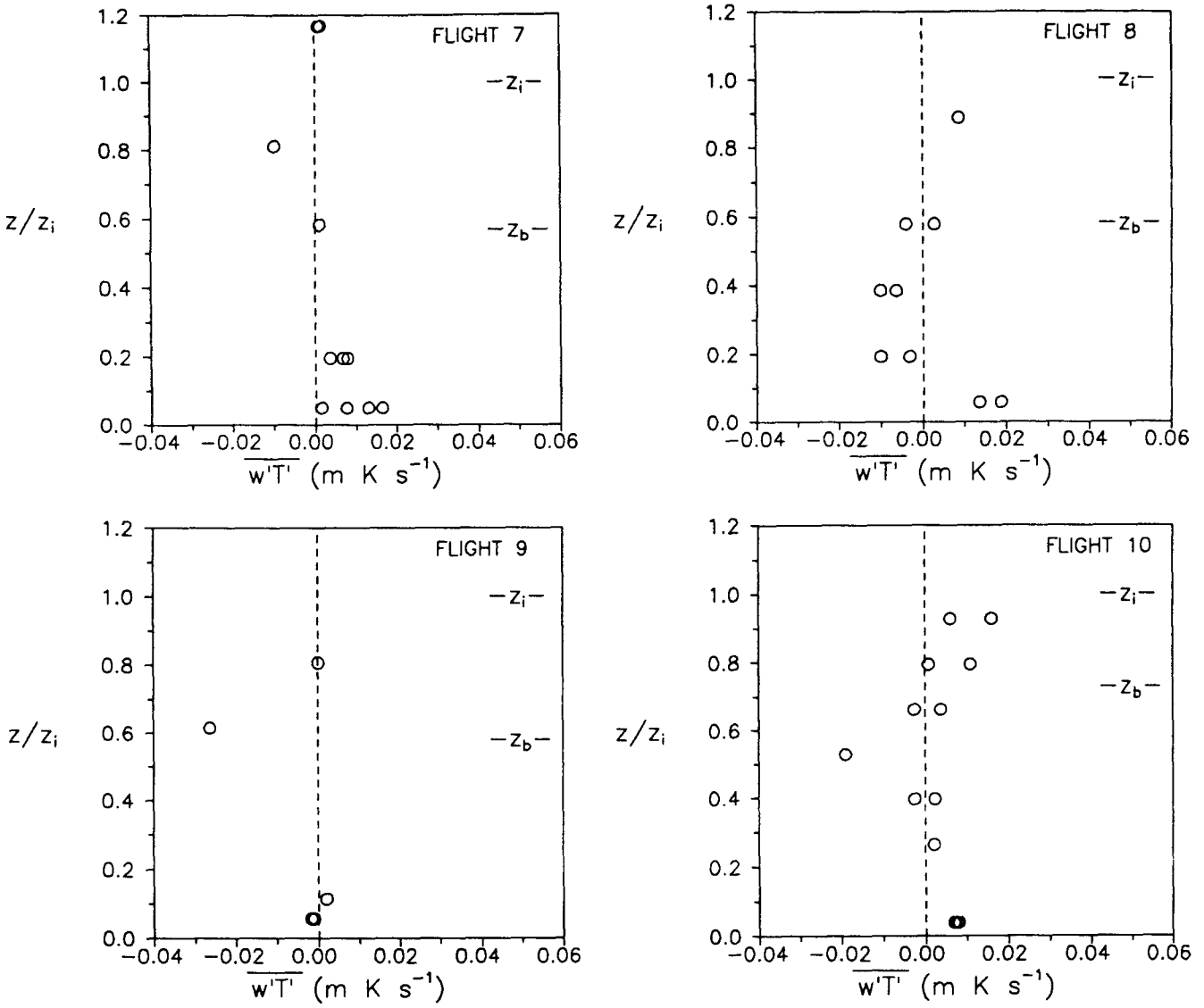

FIG. 5. Profiles of the vertical flux of temperature as a function of height divided by the boundary-layer depth observed on FIRE flights 1–10.

specific humidity measured exclusively on flights 2, 7, 8, and 9 in the vicinity of the cloud base.

Despite the presence of potential decoupling mechanisms in the form of shortwave radiation and/or precipitation on nine of the ten FIRE flights, only flights 1, 2, 9, and 10 show clear indications within their atmospheric soundings of a decoupling at cloud base (Laufersweiler and Kloesel 1991). This decoupling is readily identified by cloud-base discontinuities in both temperature and specific humidity on these four flights. The decoupling is particularly evident during the latter portion of the flights when shortwave heating of the boundary layer was nearing its peak.

With the notable exception of flight 3, observations of vertical velocity skewness, S_w, on those FIRE flights that were driven by both convection at the surface and at cloud top indicate that vertical velocity is generally positively skewed within the lower portion of the planetary boundary layer and negatively skewed within the upper portion (Moyer and Young 1991). These observations are contrary to the results of LES of stratocumulus-topped boundary layers that yield negative values of vertical velocity skewness within the lower portion of the boundary layer and positive values of S_w within the upper portion (Moeng 1986). The behavior exhibited by the vertical velocity skewness profiles modeled by the LES requires that some of the buoyant updrafts originating at the surface retain their identity up to cloud top, and conversely that some of the buoyant downdrafts generated at cloud top retain

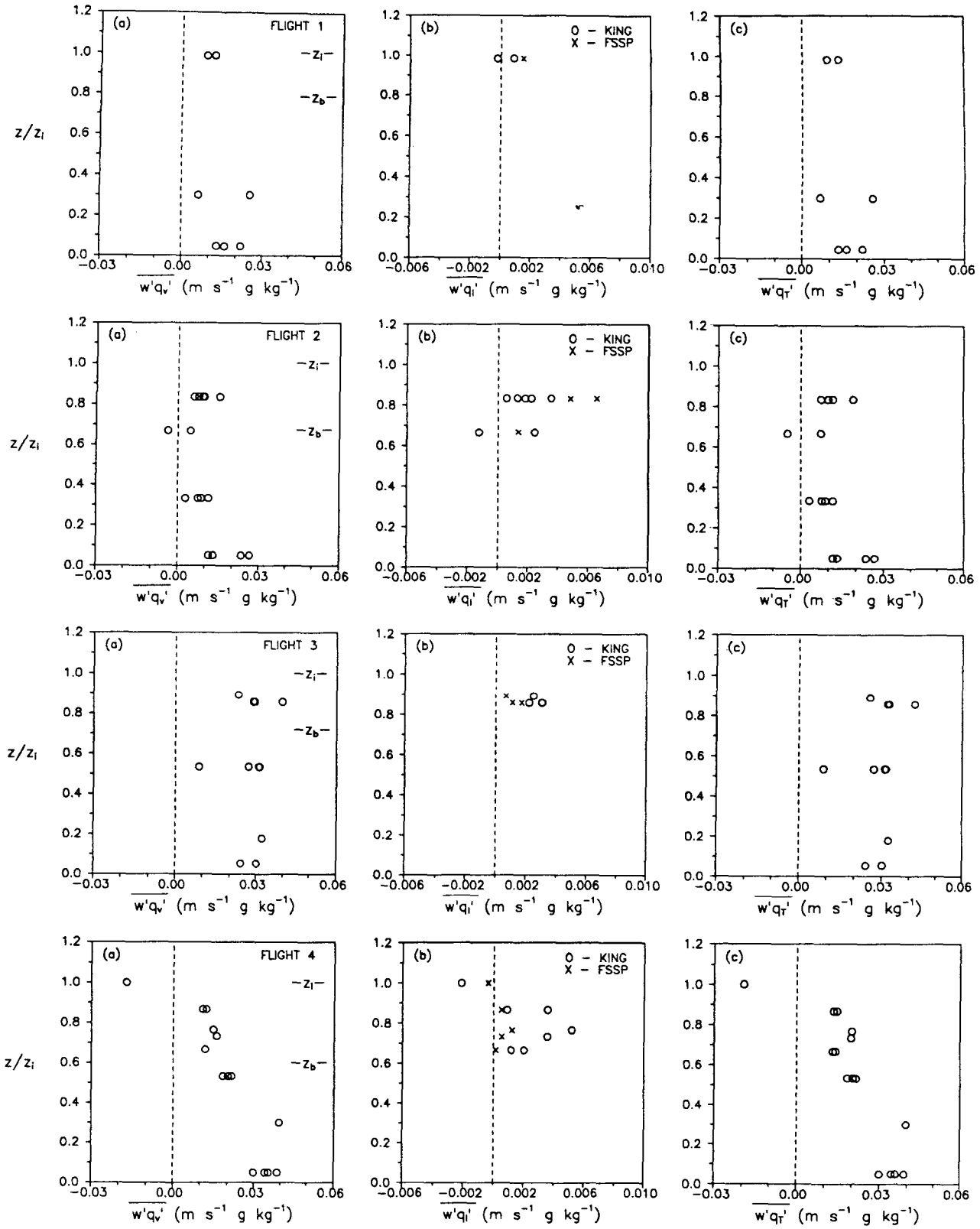

FIG. 6. Profiles of the vertical flux of water substance as a function of height divided by boundary-layer depth: (a) specific humidity flux, (b) specific liquid water flux, and (c) specific total water flux observed on FIRE flights 1–10. Note that values of $\overline{w'q_l'}$ calculated from the

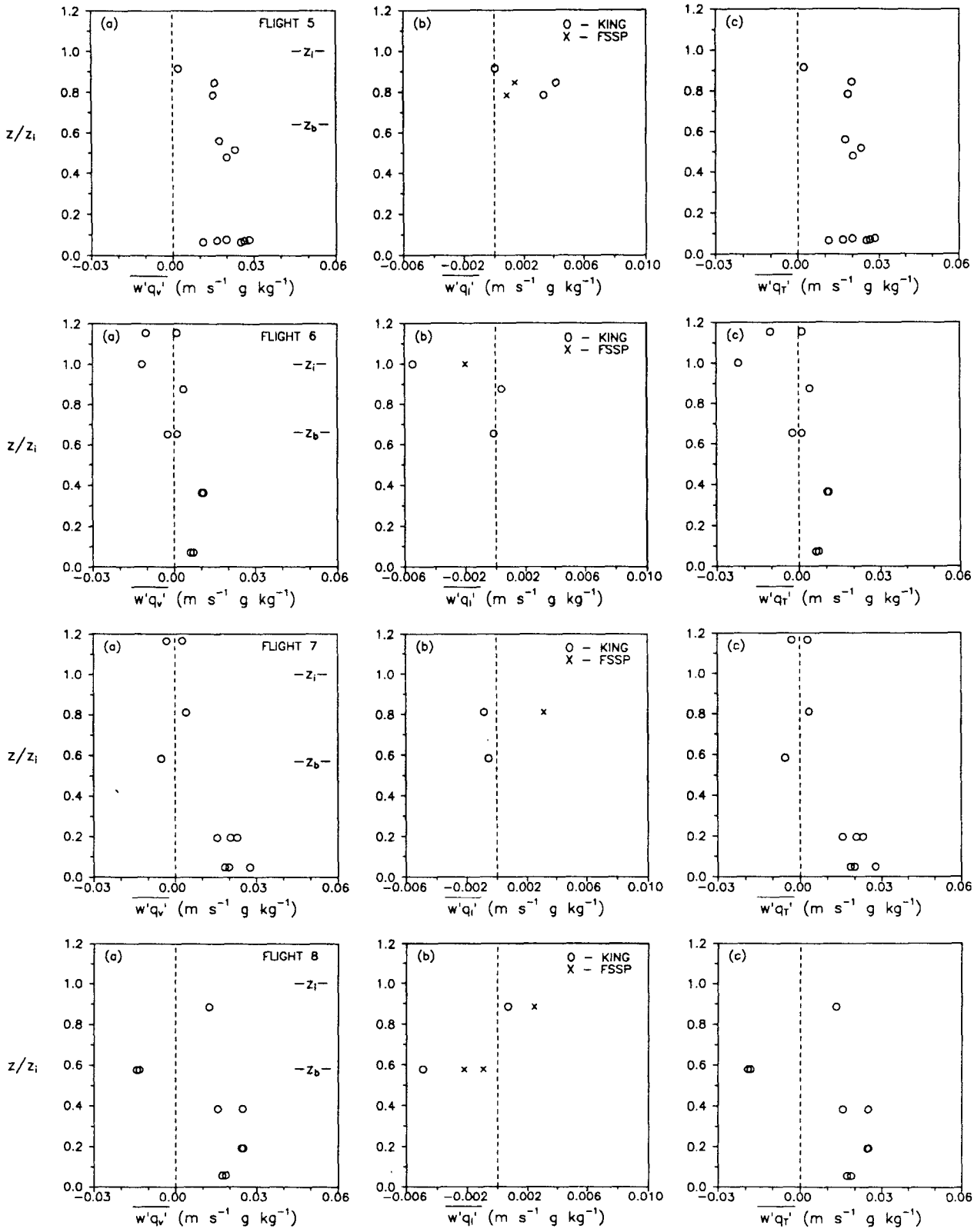

FSSP data are only displayed when a significant difference exists between these values and those values obtained using liquid water data from the King probe.

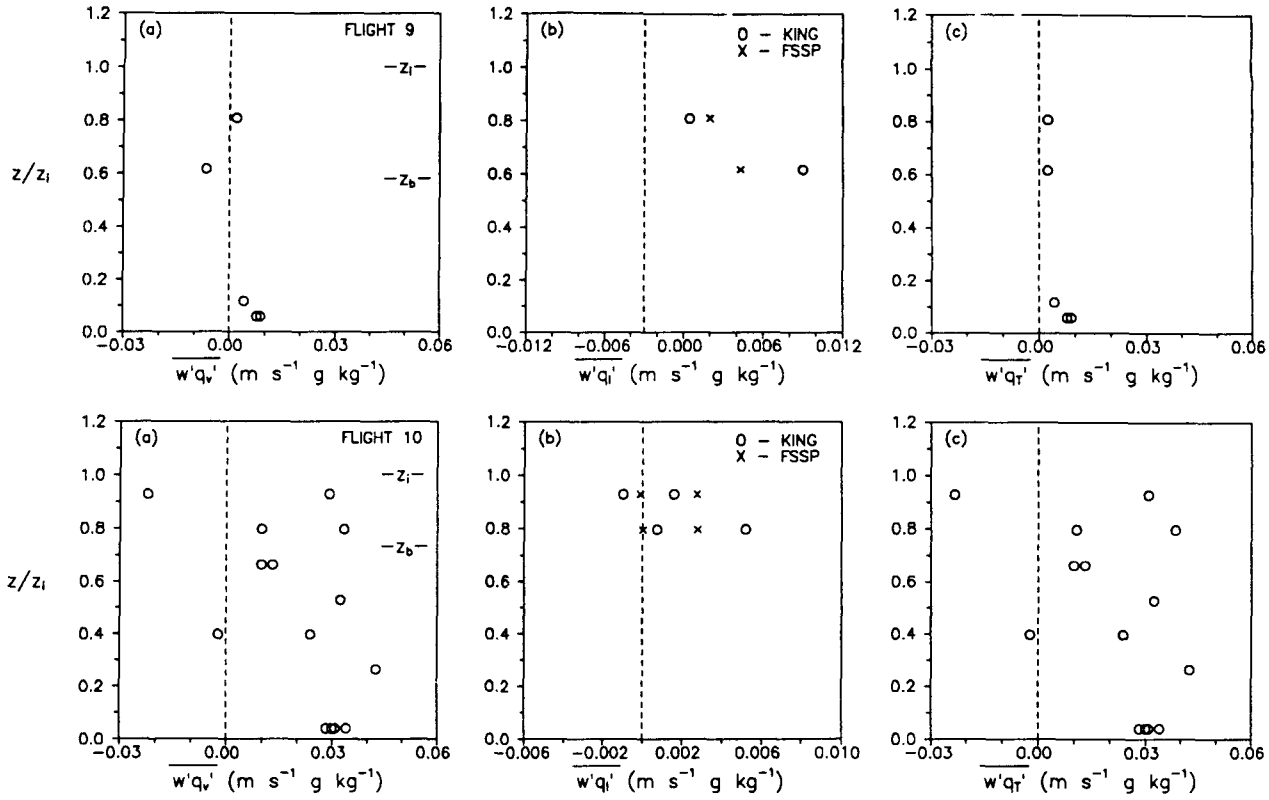

FIG. 6. (*Continued*)

their identity down to the surface (Moeng and Rotunno 1990). In contrast, the behavior exhibited by the FIRE S_w profiles (with the exception of flight 3) suggests that some mechanism was causing a reduction in the buoyancy of the turbulent plumes generated from either forcing surface as they encountered the midlevels of the boundary layer, thus prohibiting them from accelerating towards the opposite forcing surface. This observation further corroborates the existence of a stabilization near cloud base on many of the FIRE flights.

Although flight 3 exhibits a $\overline{w'T'_v}$ minimum at midlevels, it does not appear to be as distinct as most of the minima displayed on other flights. This observation is not surprising as flight 3 was a nocturnal and nonprecipitating flight and hence, was not subject to differential shortwave heating or precipitation-induced evaporational cooling near cloud base. Furthermore, flight 3 is unique among the FIRE flights in that it exhibits negative values of vertical velocity skewness (not shown) within the lower portion of the boundary layer, with a hint of positive values of S_w near cloud top. Thus, the S_w profile of flight 3 resembles the S_w profile modeled by the LES to a much greater degree than any of the other FIRE flights. This result is also to be expected because shortwave absorption and precipitation are both absent from large-eddy simulations of the stratocumulus-topped PBL. These observations, taken together, imply that differential shortwave heating and/or precipitation-induced evaporational cooling significantly reduced the buoyancy of turbulent plumes traversing cloud base in the vast majority of FIRE boundary layers, even though a decoupling of the cloud layer and the subcloud layer was not always obvious in their mean soundings.

4. Conclusions

The boundary layers investigated during FIRE span the range of buoyant forcing scenarios from nearly pure surface-forced convection through nearly pure cloud top–forced convection. A majority of the FIRE boundary layers, however, show evidence of both surface and cloud top–forced convection and thus, exhibit local maxima in buoyant forcing both near the sea surface and near the cloud top. The surface-based maximum was driven by sensible heating and/or evaporation from the sea surface, while its cloud-top counterpart was linked to positively buoyant eddies driven by radiative cloud-top cooling and/or cloud-top entrainment.

An intervening layer of near-zero or even negative values of $\overline{w'T'_v}$ is evident between the surface and cloud-top forcing regimes on many of the flights. This layer can serve as a semipermeable barrier acting to disrupt

the buoyancy of the turbulent plumes originating from either forcing regime as they traverse cloud base. Although a minimum in $\overline{w'T_v'}$ is present even in "well-mixed" cloud-topped boundary layers, it is accentuated in the presence of differential shortwave heating and/or precipitation-induced evaporative cooling, which act to stabilize the region near cloud base. On a nocturnal flight when the effects of shortwave radiation and precipitation were absent and the sole stabilizing influence was differential latent heating near cloud base, there was still evidence of a minimum in the buoyancy flux near cloud base, but the buoyancy flux remained positive, suggesting that the buoyant turbulent plumes were still able to traverse cloud base.

Although this investigation has identified some broad generalities in the buoyant forcing profiles collected during FIRE, a great deal of case-to-case variability is still in evidence. This large intercase variability is not surprising in light of the myriad of physical processes that control the structure of buoyant forcing within the marine stratocumulus-topped boundary layer. Each of these physical processes must be realistically incorporated into any model designed to accurately predict the variations in buoyant forcing that are so critical to the turbulent structure of the marine stratocumulus-topped boundary layer.

Acknowledgments. The authors greatly appreciate the technical assistance provided by B. A. Albrecht, D. H. Lenschow, and I. R. Paluch. Special thanks are also extended to M. J. Laufersweiler and K. A. Kloesel for providing the atmospheric sounding information relevant to this investigation. This research was supported by the Office of Naval Research through Grants N00014-86-K-0688 and 42418-7014.

REFERENCES

Albrecht, B. A., R. S. Penc, and W. H. Schubert, 1985: An observational study of cloud-topped mixed layers. *J. Atmos. Sci.*, **42,** 800–822.

——, D. A. Randall, and S. Nicholls, 1988: Observations of marine stratocumulus clouds during FIRE. *Bull. Amer. Meteor. Soc.*, **69,** 618–626.

Betts, A. K., and R. Boers, 1990: A cloudiness transition in a marine boundary layer. *J. Atmos. Sci.*, **47,** 1480–1497.

Brost, R. A., J. C. Wyngaard, and D. H. Lenschow, 1982a: Marine stratocumulus layers. Part I: Mean Conditions. *J. Atmos. Sci.*, **39,** 800–817.

——, ——, and ——, 1982b: Marine stratocumulus layers. Part II: Turbulence budgets. *J. Atmos. Sci.*, **39,** 818–836.

Buck, A. L., 1976: The variable path Lyman-alpha hygrometer and its operating characteristics. *Bull. Amer. Meteor. Soc.*, **57,** 1113–1118.

Deardorff, J. W., 1980a: Cloud-top entrainment instability. *J. Atmos. Sci.*, **37,** 131–147.

——, 1980b: Stratocumulus-capped mixed layers derived from a three-dimensional model. *Bound.-Layer Meteor.*, **18,** 495–527.

Kawa, S. R., and R. Pearson, Jr., 1989: An observational study of stratocumulus entrainment and thermodynamics. *J. Atmos. Sci.*, **46,** 2649–2661.

Kloesel, K. A., B. A. Albrecht, and D. P. Wylie, 1988: FIRE marine stratocumulus observations—Summary of operations and synoptic conditions. Department of Meteorology, The Pennsylvania State University, FIRE Tech. Rep. No. 1, University Park, PA, 171 pp.

Laufersweiler, M. J., and K. A. Kloesel, 1991: FIRE marine stratocumulus observations—Vertical structure of the marine atmospheric boundary layer. Department of Meteorology, The Pennsylvania State University, FIRE Tech. Rep. No. 3, University Park, PA, 153 pp.

Lenschow, D. H., I. R. Paluch, A. R. Bandy, R. Pearson, Jr., S. R. Kawa, C. J. Weaver, B. J. Huebert, J. G. Kay, D. C. Thornton, and A. R. Driedger III, 1988: Dynamics and chemistry of marine stratocumulus (DYCOMS) experiment. *Bull. Amer. Meteor. Soc.*, **69,** 1058–1066.

Lilly, D. K., 1968: Models of cloud-topped mixed layers under a strong inversion. *Quart. J. Roy. Meteor. Soc.*, **94,** 292–309.

Moeng, C.-H., 1986: Large-eddy simulation of a stratus-topped boundary layer. Part I: Structure and budgets. *J. Atmos. Sci.*, **43,** 2886–2900.

——, and R. Rotunno, 1990: Vertical velocity skewness in the buoyancy-driven boundary layer. *J. Atmos. Sci.*, **47,** 1149–1162.

Moyer, K. A., and G. S. Young, 1991: Observations of vertical velocity skewness within the marine stratocumulus-topped boundary layer. *J. Atmos. Sci.*, **112,** 403–410.

Nicholls, S., 1984: The dynamics of stratocumulus: Aircraft observations and comparisons with a mixed layer model. *Quart. J. Roy. Meteor. Soc.*, **110,** 783–820.

——, 1989: The structure of radiatively driven convection in stratocumulus. *Quart. J. Roy. Meteor. Soc.*, **115,** 487–511.

——, and J. Leighton, 1986a: An observational study of the structure of stratiform cloud sheets. Part I: Structure. *Quart. J. Roy. Meteor. Soc.*, **112,** 431–460.

——, and J. D. Turton, 1986b: An observational study of the structure of stratiform cloud sheets. Part II: Entrainment. *Quart. J. Roy. Meteor. Soc.*, **112,** 461–480.

Paluch, I. R., and D. H. Lenschow, 1991: Stratiform cloud formation in the marine boundary layer. *J. Atmos. Sci.*, **48,** 2141–2158.

Penc, R. S., and B. A. Albrecht, 1987: Parametric representation of heat and moisture fluxes in cloud-topped mixed layers. *Bound.-Layer Meteor.*, **38,** 225–248.

Pollard, R. T., 1978: The joint air–sea interaction experiment—JASIN 1978. *Bull. Amer. Meteor. Soc.*, **59,** 1310–1318.

Randall, D. A., 1980: Conditional instability of the first kind upside-down. *J. Atmos. Sci.*, **37,** 125–130.

Siems, S. T., C. S. Bretherton, M. B. Baker, S. Shy, and R. E. Breidenthal, 1990: Buoyancy reversal and cloud-top entrainment instability. *Quart. J. Roy. Meteor. Soc.*, **116,** 705–739.